ACS SENSORS

pubs.acs.org/acssensors Article

Demonstration of Selective Single-Barium Ion Detection with Dry Diazacrown Ether Naphthalimide Turn-on Chemosensors

Pawan Thapa,* Nicholas K. Byrnes,* Alena A. Denisenko, James X. Mao, Austin D. McDonald, Charleston A. Newhouse, Thanh T. Vuong, Katherine Woodruff, Kwangho Nam, David R. Nygren, Benjamin J. P. Jones,* and Frank W. Foss, Jr.*

Cite This: *ACS Sens.* 2021, 6, 192−202 Read Online

ACCESS | Metrics & More | Article Recommendations | Supporting Information

ABSTRACT: Single-molecule fluorescence imaging (SMFI) of gas-phase ions has been proposed for "barium tagging," a burgeoning area of research in particle physics to detect individual barium daughter ions. This has potential to significantly enhance the sensitivity of searches for neutrinoless double-beta decay ($0\nu\beta\beta$) that is obscured by background radiation events. The chemistry required to make such sensitive detection of Ba^{2+} by SMFI in dry Xe gas at solid interfaces has implications for solid-phase detection methods but has not been demonstrated. Here, we synthesized simple, robust, and effective Ba^{2+}-selective chemosensors capable of function within ultrapure high-pressure ^{136}Xe gas. Turn-on fluorescent naphthalimide-(di)azacrown ether chemosensors were Ba^{2+}-selective and achieved SMFI in a polyacrylamide matrix. Fluorescence and NMR experiments supported a photoinduced electron transfer mechanism for turn-on sensing. Ba^{2+} selectivity was achieved with computational calculations correctly predicting the fluorescence responses of sensors to barium, mercury, and potassium ions. With these molecules, dry-phase single-Ba^{2+} ion imaging with turn-on fluorescence was realized using an oil-free microscopy technique for the first time—a significant advance toward single-Ba^{2+} ion detection within large volumes of ^{136}Xe, plausibly enabling a background-independent technique to search for the hypothetical process of $0\nu\beta\beta$.

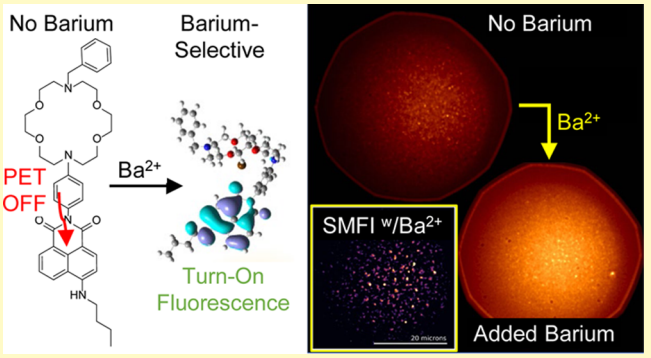

KEYWORDS: *barium tagging, barium sensor, turn-on fluorescence, PET chemosensor, single-molecule imaging*

Single-ion sensing techniques at gas−solid interfaces have the potential to enhance our structural understanding of dynamic supramolecular events on conventional solid detectors. We turned our attention to the development of functional materials for such a process when tackling one of the great open questions of particle physics,[1] whether or not the neutrino is its own antiparticle. The detection of barium daughter ions generated by double beta decay in liquid or gaseous xenon has been termed "barium tagging"[2] and is becoming a vibrant area of R&D in particle and nuclear physics.[3,4] The detection of individual Ba^{2+} ions would greatly improve detection sensitivities over background processes due to radioactivity because only the double beta decay of the ^{136}Xe isotope is expected to produce Ba^{2+} ions within a radiopure particle detector. This would enhance searches for the hypothetical radioactive process of $0\nu\beta\beta$ with a signal that is orthogonal to the radiation-based events currently measured. A robust observation would demonstrate that the neutrino is a Majorana particle—its own antiparticle—altering our understanding of neutrinos and the early history of the Universe. One possible implementation of barium tagging employs single-molecule fluorescent imaging (SMFI) with chemosensors that exhibit turn-on fluorescence in response to barium chelation.[5,6] The limited arsenal of barium sensors does not possess the proper binding and/or fluorescent characteristics necessary for SMFI at dry gas−solid interfaces. While the structural requirements for barium tagging are explored, one may envision the application of such an approach to the broader development of sensing materials at gas−solid interfaces for environmental and industrial applications.

Fluorescent chemosensors are sensitive analytical tools for rapid chemical and biochemical measurement.[7−9] Properly incorporated within SMFI experiments, they reveal individual molecular events and fundamentals, whose significance is unavailable through bulk analyses. We investigated 4-amino-

Received: October 7, 2020
Accepted: December 24, 2020
Published: January 5, 2021

https://dx.doi.org/10.1021/acssensors.0c02104
ACS Sens. 2021, 6, 192−202

1,8-naphthalimide fluorophores because they exhibit many favorable properties but have not been demonstrated for selective barium sensing.[10,11] Synthetically tractable 4-amino-1,8-naphthalimides allow construction of both photoinduced electron transfer (PET) and intramolecular charge transfer (ICT) fluorescent sensors.[12] Relatively large Stokes shifts and high photostability features are beneficial for high signal-to-noise ratios.[13] Likewise, crown ethers afford enhanced efficiency in binding to metal ions and can act as switches for PET- and ICT-based sensors without the need for proton transfer or metal ion exchange that renders other molecules useless in solventless environments.[14] As such, 4-amino-1,8-naphthalimide fluorophores with crown ether-based binding domains have been used as colorimetric and fluorescent sensors for the detection of ions and small molecules that are of great significance to the environment, human health, and industrial processes.[15−18] Several 4-amino-1,8-naphthalimide chemosensors have been developed for detection of cations, anions, and small polar molecules.[19−22] However, chemosensors with selective response to Ba^{2+} remain underdeveloped.[9,23]

Selective barium sensing has been demonstrated by a relatively small number of fluorescent chemosensors.[9,24−32] This is not surprising because barium sensing is not widely studied for clinical or environmental reasons; although acute barium exposure can be deadly, diagnoses are rare and often confirmed by inductively coupled plasma mass spectrometry analysis of the patient's plasma and urine.[33,34] Nakahara and co-workers pioneered a monoazacryptand receptor with a PET switch to pyrene fluorescence that operates in aqueous micellar systems and would require relatively high-energy excitation that would make SMFI challenging in our system.[35−37] Crown ether systems have invoked termolecular complexes with two crown moieties sandwiched around one Ba^{2+}, which would also be limited in dry-phase sensing, where bimolecular interactions may be preferred.[23,38] A bioinspired G-quadruplex chemosensor provided rapid detection of Ba^{2+}, also in solution.[39,40] Recently, a fluorescent chemosensor based on the phenoxazine system with an ICT turn-on mechanism was reported for Ba^{2+}, where charge transfer was achieved by metal binding specifically to a single amide functional group.[41] These receptors are instructive but unsuitable for long-term dry-phase SMFI device design, presumably as part of a functional monolayer or thin coating deposited on a translucent optical device.

Within the context of R&D toward a barium-tagging phase of the NEXT program's search for $0\nu\beta\beta$ decay,[42−44] we previously demonstrated single-ion sensitivity to Ba^{2+} using commercial chemosensors in an aqueous suspension.[4] Achieving single-ion sensitivity mandated the use of the competitive binding agent BAPTA and used fluorophores incompatible with dry operation. To address the challenge of solventless sensing of barium, we demonstrated a class of dry-phase active fluorescent chemosensors using monoazacrown receptors.[37] Single-molecule sensitivity of this system[37] was elusive because of UV excitation of impurities in the substrates and a lack of photobleaching transitions to use for single-molecule identification. Similar molecules were then recently shown to be suitable for ratiometric or "bicolor" Ba^{2+}-sensitive fluorescence,[45] a promising new direction under consideration for barium tagging.

In this paper, we report a study on the synthesis, characterization, analysis, and computational modeling of a new family of monoazacrown ether and diazacrown ether naphthalimide fluorescent sensors (Figure 1) with enhanced selectivity and sensitivity to Ba^{2+}. These visible fluorescent probes are amenable to SMFI microscopy in dry environments and consequently allowed us to resolve individual Ba^{2+} ions without a competitive binding agent. This improves upon our initial sensor dyes,[37] with visible excitation proving to be a critical ingredient in overcoming fluorescent backgrounds of glass and quartz substrates at the level required for single-molecule sensitivity. We also report on computational models that offer reliable predictability of target ion- and binding site-dependent fluorescent response within this family, a capability that will accelerate explorations of structure−function relationships in future dry-phase SMFI probes.

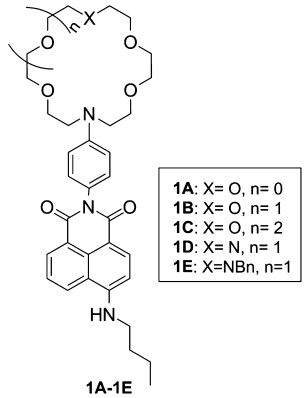

Figure 1. Napthalimide derivatives used in this study.

EXPERIMENTAL SECTION

Synthesis. The synthesis of naphthalimide derivatives **1A−1E** is shown in Scheme 1. Monoazacrown ethers **2A−2C** were assembled as previously described.[37,46] Diaza-18-crown-6 ethers were prepared by the modification of methods from a previous report.[47] Complete details and full chemical characterization can be found in the Supporting Information.

Sample Preparation for Solution-Phase Studies. Stock solutions of probe molecules were prepared at 1×10^{-3} M concentration in an acetonitrile solvent. Stock solutions of metal perchlorates were made at 1×10^{-2} M concentration in a 9:1 acetonitrile/water mixture. UV−vis studies were performed with and without Ba^{2+} in acetonitrile, dichloromethane, acetone, and ethanol solvents with probe **1B** (10×10^{-6} M) and barium perchlorate (50×10^{-6} M). Fluorescence titration and metal ion selectivity studies were performed by maintaining a final concentration of the probe molecule at 1×10^{-6} M concentration. Metal ion selectivity studies were conducted by maintaining metal perchlorate concentrations at 5×10^{-6} M. Competitive fluorescence experiments were performed using 2×10^{-6} M probe **1D** with 5×10^{-6} M metal perchlorate solution in an acetonitrile solvent. Job's plot experiments were performed by maintaining a total concentration of the probe and barium perchlorate solution at 20×10^{-6} M. Samples were incubated for 2 min in the dark before measuring fluorescence intensity. ^{1}H NMR titration experiments were conducted with the concentration of the probe at 1×10^{-2} M and metal perchlorate (barium, potassium, and mercury) at 1×10^{-2} and 5×10^{-2} M in an acetonitrile-d_3 solvent at room temperature.

Slide Preparation for Dry-Phase Fluorescence. Dry samples of probe **1D** on glass slides for dry-phase fluorescence studies were prepared as follows: an acetonitrile solution of barium-selective probe **1D** was mixed into cyanoacrylate in 1:1 ratio to desired concentration (10×10^{-12} to 10×10^{-6} M). A total of 30 μL of this solution was applied to a glass microscope slide and then dried in an oven for 5

https://dx.doi.org/10.1021/acssensors.0c02104
ACS Sens. 2021, 6, 192−202

Scheme 1. Synthesis of 4-Amino-1,8-naphthalimide Sensors

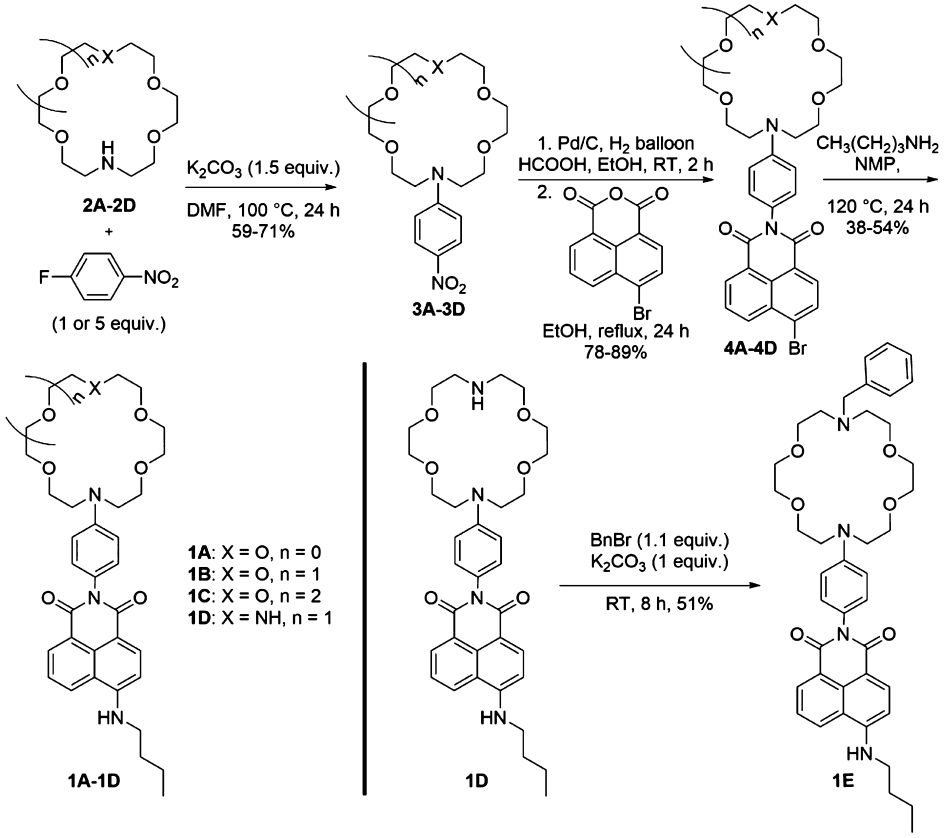

min at 373 K to set it into a thick solid layer. Fluorescence response from three slides was measured with excitation at 430 nm before and after washing with 50 μL of 1 × 10^{-3} M metal perchlorate in acetonitrile or only acetonitrile and then drying. Each slide was then rescanned three times, and the fluorescence response was averaged to yield a mean response.

Microscopy Details. Probe **1D** was suspended at a concentration of 10^{-11} M within the cyanoacrylate matrix and analyzed via fluorescence microscopy. Excitation is delivered with a supercontinuum laser with the output selected using an acousto-optical tunable filter. For the studies performed here, several output lines were superposed between 420 and 437.5 nm, to maximize output power and cover the excitation band of **1D**. Laser light was cleaned by passing through a beam expander and cutting off the outer, nonuniform edge with an iris, generating a circular and approximately Gaussian beam profile. The beam was then redirected through a 500 nm short-pass filter to reduce incident background light, reflected off a 505 nm dichroic mirror, and focused through a 100× air-coupled microscope objective (NA = 0.95) for a final power output of 125 mW to excite the **1D** matrix in the epifluorescent mode. The objective collected resultant Stoke's shifted fluorescent emissions, which were then passed back through the dichroic mirror and a 500 nm long-pass filter, again for background reduction, and collected via a Hamamatsu EMCCD camera, which acquired one image every half second into 300-image sequences.

Microscopy images were processed using an algorithm that first filters the image in Fourier space to remove slowly sloping backgrounds and then sums the sequence over the full imaging time. After filtering, single-molecule candidates can be identified after subtracting the background profile, which is found by blurring the summed image via a Gaussian filter. Single-molecule candidates are identified as points with intensities in the excess of 3σ above the background. Once the candidates are identified, their locations on the raw images are analyzed as a function of time for the duration of the sequence to produce fluorescent trajectories. These trajectories are scanned for an instantaneous drop or "single-step" profile, which is the hallmark characteristic of a single molecule undergoing a discrete photobleaching process.

Computation Details. Molecular structures were optimized using the M06-2X[48] functional with the SDD[49−52] effective core potential basis set for heavy metal atoms (barium and mercury) and def2-SVP[53,54] basis set for other atoms, followed by frequency analysis to confirm the nature of their energy minima (no imaginary frequency). Calculations with time-dependent density functional theory (TDDFT)[55] were carried out to reveal the orbitals involved in the observed fluorescence events. SMD[56] or PCM[57] solvation models were used to incorporate solvent effects with acetonitrile as the solvent. All calculations were performed using the Gaussian 09 program.[58]

RESULTS AND DISCUSSION

Synthesis. Scheme 1 represents the synthesis of probes **1A−1E**. In brief, nucleophilic aromatic substitution of 4-fluoronitrobenzene by mono/diaza crown ethers, prepared by modification of our previous work,[37] gave the desired 4-nitroaniline derivatives **3A−3D**. Reducing 4-fluoronitrobenzene to one equivalent was critical in the case of diaza-18-crown-6 ether **2D**. Nitro reduction by Pd-catalyzed hydrogenolysis followed by condensation with commercially available 4-bromonaphthalic anhydride resulted in the desired bromonaphthalimide products **4A−4D**. Initial attempts for the final nucleophilic aromatic substitution reaction of bromonaphthalimide with *n*-butylamine in 2-methoxyethanol led to poor yields of the desired aminonaphthalimides. However, switching the solvent to *N*-methyl-2-pyrrolidone, a basic solvent, enabled the bromide substitution to afford the desired aminonaphthalimides **1A−1D**. Compound **1E** was prepared by nucleophilic substitution by dropwise addition of benzyl

https://dx.doi.org/10.1021/acssensors.0c02104
ACS Sens. 2021, 6, 192−202

bromide into a solution containing **1D** and potassium carbonate. Overall, this synthetic approach led to the efficient preparation of the desired naphthalimide fluorescent probes **1A**−**1E**.

UV−Vis Studies. UV−vis spectra of all synthesized 1,8-naphthalimide-based fluorescent probes (**1A**−**1E**) were recorded in an acetonitrile solvent at room temperature. Major absorbances were centered between 200−300 and 380−480 nm—consistent with 4-amino-1,8-naphthalimide chromophores.[11] Solutions doped with Ba^{2+} provided no or negligible shifts on UV−vis absorbances in all probes (Figure S11). These effects were also encountered in acetone and ethanol (Figure S12). In dichloromethane, however, a slight red shift was observed possibly because of change in solvent polarity as a result of addition of barium ions in the acetonitrile solvent. $Ba(ClO_4)_2$ addition led to a concentration-dependent increase in fluorescence centered near 530 nm in probes **1B**, **1D**, and **1E**, when excited at λ_{max} obtained from the UV−vis spectrum, suggesting turn-on fluorescence by changes to PET.[17] Similarly, fluorescence analysis as a function of absorption wavelength from 430 to 460 nm showed no significant change in the emission intensity profile (Figure S13).

Fluorescence Response and Metal Ion Selectivity. Fluorescent response to cationic analytes was determined for each of the synthesized probes (1.0 μM in acetonitrile). Stock solutions of perchlorate salts were prepared in a 9:1 mixture of $MeCN/H_2O$ to achieve complete dissolution. The final concentration of the perchlorate solution was maintained at 5 μM to achieve 1:5 concentration ratio of the probe to the ion analyte. The selectivity studies are summarized in Figure 2, top

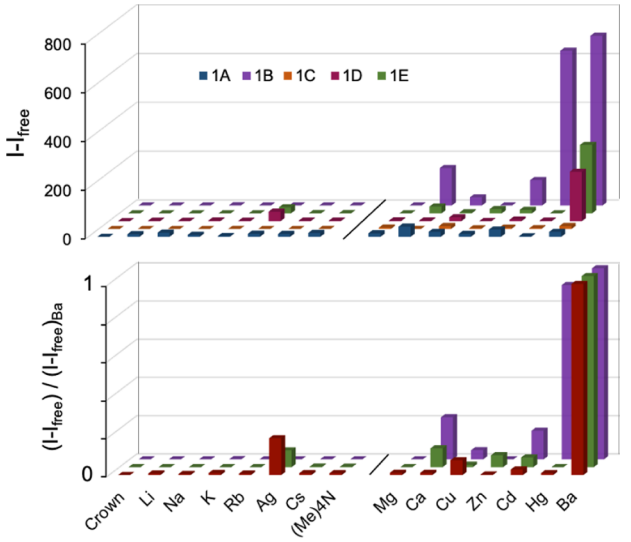

Figure 2. Top: ion perchlorate (5×10^{-6} M) response to **1A**−**1E** (1×10^{-6} M) in MeCN solution. Bottom: fluorescence response of **1B**, **1D**, and **1E** with different cation solutions normalized to fluorescence intensity for barium perchlorate.

panel with emission at 530 nm. Figure S20 demonstrates I/I_0 analysis of the same data. Molecular probes 1A and **1C** were not effective optical sensors for almost all tested ions. A small twofold response was found in the case of calcium with probe 1A. In contrast, **1B** showed excellent sensitivity toward Ba^{2+} and Hg^{2+} in addition to a lesser response to Ca^{2+}. In the presence of Ba^{2+} and Hg^{2+} solutions, ca. 30-fold increases in fluorescence intensities were observed. Ca^{2+} and Cd^{2+} ions also showed eightfold and fivefold increases, respectively, for probe **1B**.

Two novel 4-amino-1,8-naphthalimide derivatives containing diazacrown ether-binding domains **1D** and **1E** were found to have excellent selectivity to Ba^{2+}. **1D** and **1E** showed solution-phase emission enhancements of 11-fold and 22-fold, respectively, in the presence of Ba^{2+}. Among the different ions (Mg^{2+}, Ca^{2+}, Cu^{2+}, Zn^{2+}, Cd^{2+}, Hg^{2+}, Ba^{2+}, Li^+, Na^+, K^+, Rb^+, Ag^+, Cs^+, and $(CH_3)_4N^+$) studied, only Ba^{2+} showed significant increased fluorescence for probes **1D** and **1E**. Other ions showed little to no (<2×) fluorescence intensity. Normalized fluorescence responses highlight selectivity by ignoring differences in absolute brightness and show **1D** and **1E** with highest selectivity for Ba^{2+} (Figure 2, bottom panel).

Barium sensitivity remained in all but one competitive fluorescence experiment (Figure 3). The barium selectivity of

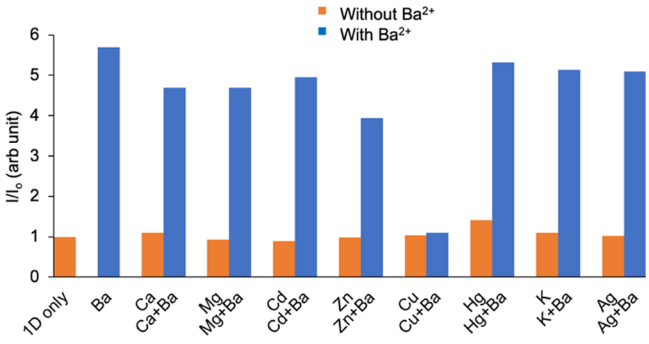

Figure 3. Fluorescence response of **1D** (2×10^{-6} M) to Ba^{2+} (5×10^{-6} M) in the presence of other metal ions (ions, 5×10^{-6} M) in acetonitrile. Slit width 2.5/5.0.

probe **1D** is observed in all cases, except for open-shell Cu^{2+}. Cu^{2+} addition showed a blue-shifted absorption spectrum reminiscent of the aminoless 4-*H*-naphthalimide chromophores (Figure S21). This phenomenon is potentially due to Cu^{2+}'s strong binding to the 4-amino-residue, truncating the cross-conjugation of the sensor chromophore of **1D**. However, Cu^{2+} and other open-shell transition metals often interact with PET fluorophores to quench fluorescence by an electron/energy transfer mechanism.[59,60] This effect was observed in another "turn-off" Cu^{2+} 4-amino-1,8-naphthalimide sensor.[61] We compared the fluorescence of Cu^{2+} and Ba^{2+} addition to the sensor **1D** and to a binding domain-free 4-amino-1,8-naphthalimide analogue (**Fluo**, Figure S22). Cu^{2+} effects were identical with and without the crown ether moiety. DFT computational studies have limitations for such open-shell systems,[62] but our studies were consistent with these Cu^{2+} experimental results, showing an open-shell nonfluorescent **1D** molecule and interactions with the 4-amino residue in our model fluorophore (**Fluo**, Figure S23). Despite the interesting copper inactivation, these data are evidence of increased sensor selectivity of two novel turn-on optical sensors **1D** and **1E** to Ba^{2+}.

Fluorescence Titration and Binding Studies. Fluorescence titration curves presented in Figures 4A, S14A, and S15A show that the emission reaches maxima near one equivalent of Ba^{2+} addition for probes **1E**, **1B**, and **1D**, respectively. Titration studies performed with probes **1B**, **1D**, and **1E** with an increasing concentration of barium perchlorate in acetonitrile gave dissociation constant values (k_d) of 0.72×10^{-6}, 0.59×10^{-6}, and 0.75×10^{-6} M, respectively. These low

https://dx.doi.org/10.1021/acssensors.0c02104
ACS Sens. 2021, 6, 192−202

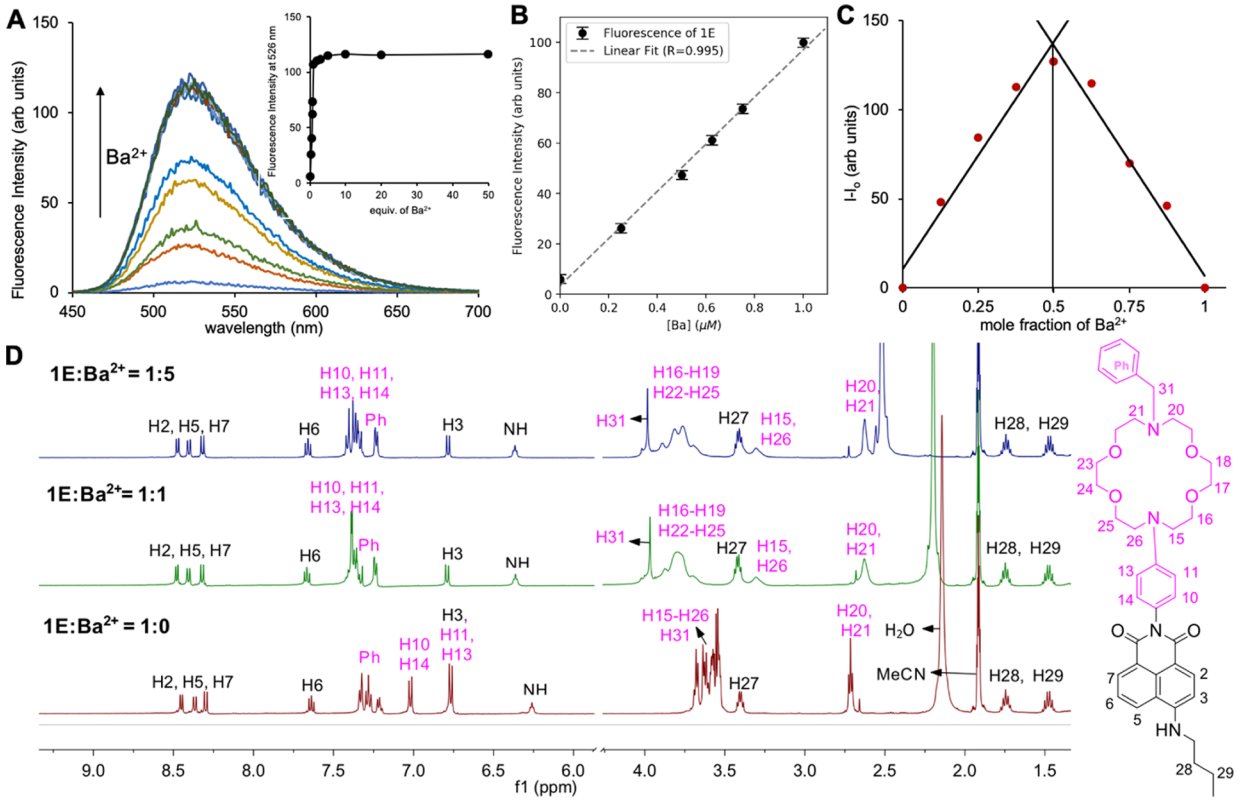

Figure 4. (A) Fluorescence titration spectra of **1E** (1×10^{-6} M) upon addition of $\mathbf{Ba}^{2+}$ (0 to 50×10^{-6} M) in acetonitrile (λ_{ex} = 430 nm). (B) Linearity of fluorescence intensity at 526 nm for **1E** (1×10^{-6} M) in acetonitrile as a function of the concentration of $\mathbf{Ba}^{2+}$. (C) Job's plot figure for **1E**−$\mathbf{Ba}^{2+}$ at constant total concentration 20×10^{-6} M of **1E** and barium in acetonitrile. (D) ^{1}H NMR titration spectra of probe **1E** with the addition of 0.0 (red trace), 1.0 (green trace), and 5.0 (blue trace) equiv of Ba^{2+} in acetonitrile-d_3. The inset shows the plot of fluorescence change as a function of $\mathbf{Ba}^{2+}$ concentration. Slit width 2.5/5.0.

dissociation constants reveal effective binding between each probe and Ba^{2+}. Solution-phase limits of detection (LOD) were calculated using linear fitting curves of fluorescence titration data and the formula LOD = $3\sigma/k$, where σ is the standard deviation of the blank sample without barium and k is the slope between intensity versus barium concentration,[63] resulting in 0.0288×10^{-6}, 0.074×10^{-6}, and 0.006×10^{-6} M detection limits for probes **1E**, **1B**, and **1D**, respectively. Figures 4B, S14B, and S15B show good linear correlation for probes **1E** (R^2 = 99.5), **1B** (R^2 = 98.5), and **1D** (R^2 = 99.1). Overall results show that the probes **1B**, **1D**, and **1E** can detect Ba^{2+} in solution at nanomolar concentrations and therefore can be highly practical fluorescent sensors for selective detection of Ba^{2+}. The stoichiometry of binding for molecular probes **1B** and **1E** with barium was calculated by Job's method. The results, presented in Figures S14C and 4C, show the inflection point of two linear fitting curves at 0.46 and 0.50 mol fraction for complex **1B**−$\mathbf{Ba}^{2+}$ and **1E**−$\mathbf{Ba}^{2+}$, respectively. This indicates a 1:1 binding stoichiometry between probes **1B** and **1E** with Ba^{2+}. Additionally, complex **1B**−$\mathbf{Ba}^{2+}$ was observable in high-resolution mass spectrometric analysis of solution of **1B** and barium perchlorate (Figure S14D).

^{1}H NMR Studies. Complexation between Ba^{2+} and fluorescent probes **1B**, **1D**, and **1E** was further demonstrated by ^{1}H NMR experiments performed with 1:1 and 1:5 M ratios of the probe and $Ba(ClO_4)_2$ in acetonitrile-d_3. Ba^{2+} addition resulted in downfield shifts of *N*-phenyl-aza crown ether protons, while the chemical shift values of protons in the naphthalimide fluorophore group have minimal or no change (Figure 4D). Noticeably, an upfield shift in α-protons of the anilino nitrogen in azacrown ether was also observed (H15 and H26 in Figure 4D) in all molecular probes (for **1B** and **1D**, see Figure S16), suggesting that the nitrogen atom of *N*-phenyl-aza crown ether was not directly involved in ion binding. Similarly, the effect of Ba^{2+} on the *N*-benzyl group in probe **1E** was observed, as seen with downfield shifts of both aromatic and benzylic protons (Figure 4D). Additionally, in fluorescent probes **1D** and **1E**, all α-protons of two nitrogen atoms in the diazacrown ether structure showed an upfield shift, indicating no interaction between both the nitrogen atom of diazacrown and Ba^{2+}. The results obtained from ^{1}H NMR experiments with probes clearly show the binding of Ba^{2+} on the receptor crown ether units with no significant binding on naphthalimide fluorophore units. Comparative ^{1}H NMR studies were carried out with Ba^{2+}, Hg^{2+}, and K^+ in the case of probe **1B**, which showed distinct features in the NMR spectra. With Hg^{2+} addition, all monoazacrown methylene protons were deshielded, indicating binding of the nitrogen atom of *N*-phenyl-aza crown ether with Hg^{2+} (Figure S17). With K^+, however, no observable change was found in the chemical shift values of the protons of both naphthalimide and azacrown ether moieties (Figure S18).

Computational Studies. Computational models were studied using TDDFT to predict the fluorescence behavior of sensors in response to ions as calculated within an acetonitrile solvent model (Figure 5A−D) As a test suite, we considered molecules **1B** and **1E**, both unchelated and chelated with Ba^{2+}, K^+, and Hg^{2+}. The results support the

https://dx.doi.org/10.1021/acssensors.0c02104
ACS Sens. 2021, 6, 192−202

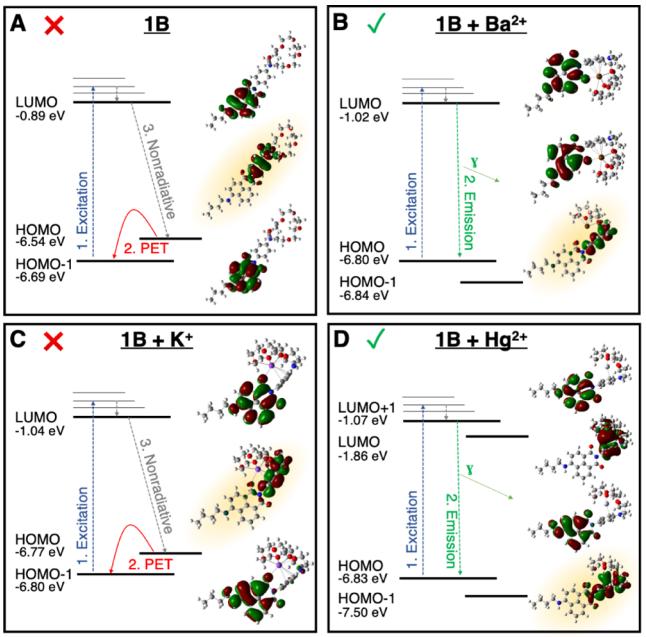

Figure 5. Simulated orbitals of **1B**. The mechanism of PET and CHEF is illustrated by the change in energy of the nitrogen-dominated orbital, highlighted, upon binding various cations.

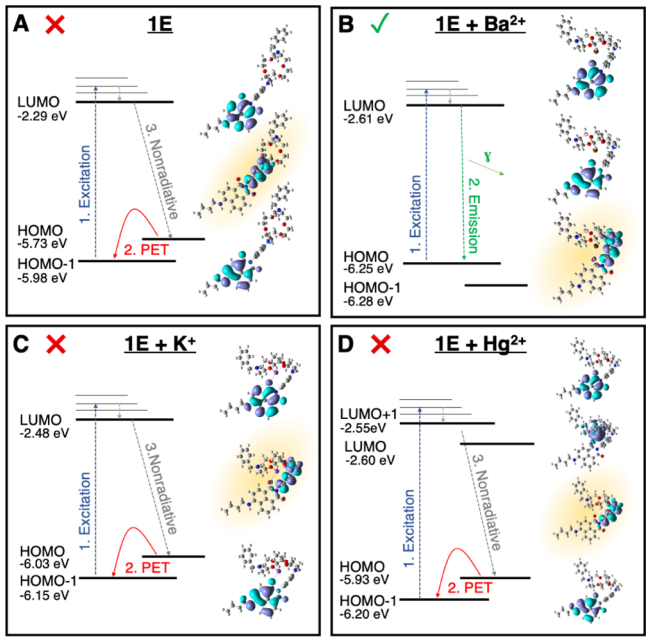

Figure 6. Simulated orbitals of **1E**. Enhanced Ba^{2+} selectivity is illustrated by comparing changes in energy of the nitrogen-dominated orbital, highlighted.

proposed PET-mediated off-state within unchelated mono- and diazacrown ether naphthalimides, which is turned on by chelation-enhanced fluorescence (CHEF) upon ion binding. In the unbound **1B** species (Figure 5A), excitation of the naphthalimide fluorophore is governed by a HOMO−1 to LUMO transition based on orbital analysis. The electrons in the interstitial $HOMO_{free}$ orbital of the receptor (highlighted) are localized around the *N*-aryl unit and energetically well positioned to quench the excited state before fluorescence transition can occur from the LUMO to HOMO−1, by a traditional PET mechanism. Upon barium chelation, however, the $HOMO_{free}$ level is drastically stabilized by mixing with Ba^{2+} and becomes the new HOMO−1 (Figure 5B), allowing the fluorophore-centered HOMO and LUMO levels of the barium bound species to participate in fluorescence without PET quenching.

As **1B** responds to Hg^{2+} but not to K^+, we examined the arrangement of frontier molecular orbitals when complexed to these cations. Chelation is effective and lowers the critical PET-enabling $HOMO_{free}$ orbital through binding to both ions. However, in the case of K^+, PET quenching is still possible (Figure 5C), predicting a nonfluorescence response to K^+ consistent with the experiment. Hg^{2+} chelation results in notable lowering of the HOMO, LUMO, and LUMO+1 energy states relative to the free chemosensor (Figure 5D); the LUMO and LUMO+1 states show substantial lowering in energy including a reordering of states, not unusual among heavy-atom binding.[64] Excitation of the fluorophore-centered electrons (HOMO to LUMO+1) is not quenched by PET. Thus, CHEF occurs with Hg^{2+} addition to **1B**, similar to the barium chelation, albeit with a different rearrangement of orbital energies.

Analysis of the selective diazacrown ether chemosensor **1E** showed similarity to **1B** when free and bound to Ba^{2+} and K^+, especially with respect to the critical relative location of the $HOMO_{free}$ orbital (highlighted in Figure 6). However, Hg^{2+} binding resulted in a weaker effect on the $HOMO_{free}$ orbital, and the fluorescence of Hg^{2+}-bound species is still quenched by internal PET from the HOMO to HOMO−1. Overall, the theoretical studies support experimental results for the enhanced selectivity of **1E** to Ba^{2+}.

In conclusion, the theoretical models correctly predict the observed switch-on fluorescence patterns across all ions and species tested. These are summarized in Table 1.

Table 1. Summary of Computational Results Compared with Experimental Observations of Switch-On Fluorescence

probe	ion	fluorescence predicted	fluorescence observed
1B		no	no
1B	Ba^{2+}	yes	yes
1B	K^+	no	no
1B	Hg^{2+}	yes	yes
1E		no	no
1E	Ba^{2+}	yes	yes
1E	K^+	no	no
1E	Hg^{2+}	no	no

Dry SMFI of Ba^{2+}. To demonstrate single-ion sensing in a dry environment, compound **1D** was suspended in a cyanoacrylate polymer. Polyvinylacetate and polystyrene matrices were initially investigated with interesting yet relatively poor solvochromatic effects on bulk fluorescence. Barium-induced fluorescence was first verified by spectrophotometry in a bulk matrix. A strong fluorescent response was observed across all three tested locations on three slides, although with significant variability observed because of the imperfect uniformity of layer deposition. Figure 7A shows the background-subtracted response of slides with no added Ba^{2+} and after Ba^{2+} wash. Fluorescence is normalized to activity on the rising edge of the excitation peak before background subtraction. Mean and standard deviation are shown as dashed and filled regions, in addition to individual response curves.

https://dx.doi.org/10.1021/acssensors.0c02104
ACS Sens. 2021, 6, 192−202

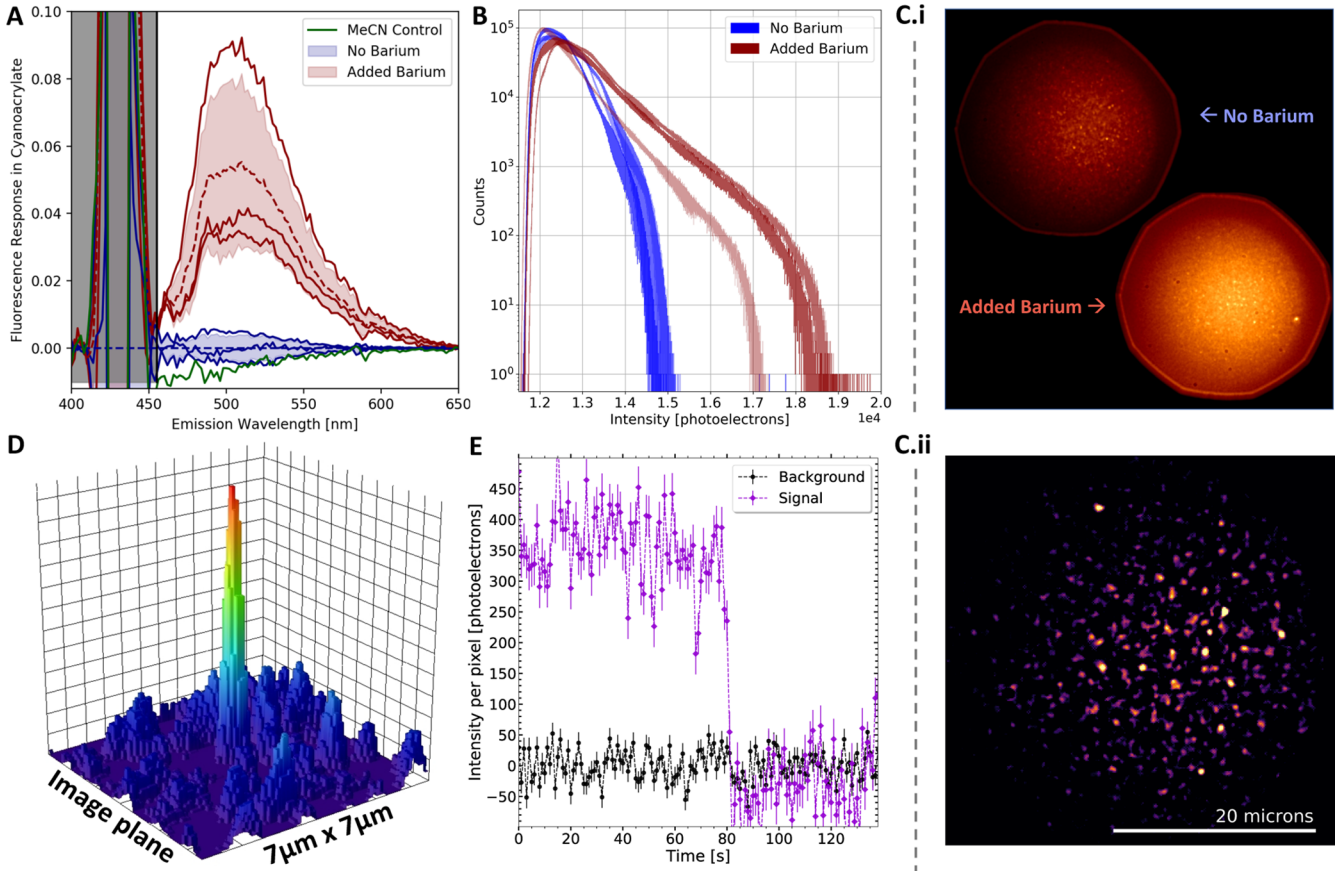

Figure 7. Solid-matrix measurements of barium-sensing fluorophore **1D**. (A) Bulk spectrophotometry in a dried cyanoacrylate matrix; (B) raw pixel histogram of three **1D**-coated slides imaged at the single-molecule level; (C) single-molecule level microscopy images of the **1D** layer with and without Ba^{2+} (i) and with Ba^{2+} after background removal (ii); (D) specific single reconstructed barium-chelated **1D** molecule; and (E) barium-chelated **1D** molecule fluorescence time trajectory showing a single-step photobleaching characteristic of SMFI detection.

Also, the shown overlaid is a control measurement using a pure solvent wash, resulting in slightly reduced fluorescence, likely because of removal of some ionic contamination or fluorescent emitters from the surface. Furthermore, the selectivity toward barium is maintained in the dry phase because this fluorescent response was not observed in the case of potassium and mercury (Figure S19). These data demonstrate that fluorescent response to Ba^{2+} is maintained in the dry phase, as observed in our past work with molecules of this family,[37] however, now with selectivity for barium ions and the potential for enhanced SMFI.

The imaging modality for SMFI in this paper is air-coupled epifluorescent microscopy. This too is distinct from our prior work[4] on SMFI imaging of Ba^{2+} in solution, which used total internal reflection fluorescence (TIRF). TIRF offers combined benefits of a reduced background by exciting only at the glass−sample interface and oil couplings that allow for high numerical aperture imaging. The oil required for through-objective TIRF, however, is likely problematic within the high-purity xenon environment of our target application. Because the oil-free imaging modality used here introduces additional practical challenges, realization of single-Ba^{2+} imaging in this way encapsulates an important practical step toward application in time projection chambers.

A set of slides was prepared for single-ion level imaging of barium, with compound **1D** suspended at 10 pM concentration in the cyanoacrylate matrix. Slides were washed with a 1 nM Ba^{2+} solution. A stark increase in the net fluorescence intensity of the sample was observed upon addition of Ba^{2+}. Three slides were tested, with image sequences taken across three locations both before and after the barium solution was introduced. The increase in intensity was quantified via a raw pixel histogram for each slide, as shown in Figure 7B. A robust increase in bright pixels was observed in all cases, indicative of turn-on fluorescence.

The detected fluorescence in these images originates from molecules at various distances from the focal plane, with near-focus points appearing very bright and out-of-plane candidates appearing dimmer. Both before and after addition of Ba^{2+}, an array of spots of various degrees of brightness can be observed, undergoing discrete photobleaching transitions over time, with the number dramatically enhanced in the barium-added images. An example of a before/after comparison is shown in Figure 7C(i), where in both cases, bright points corresponding to distinct barium−**1D** complexes can be visually identified.

Using a sample with 10 pM barium perchlorate solution applied to the 10 pM sensor matrix, the interpretation of these bright emitters as single molecules was confirmed. Figure 7C(ii) shows an example image processed and filtered according to the algorithm described in the Microscopy Details section, which is used as an input to time series analysis. The well-localized candidate spots in this image, an example of which is shown isolated in Figure 7D, are observed to exhibit discrete photobleaching transitions, as shown in Figure 7E. This behavior, also observed visually for the bright

https://dx.doi.org/10.1021/acssensors.0c02104
ACS Sens. 2021, 6, 192−202

spots in the denser samples, as well in previous work in the solution phase,[4] confirms the single-molecule interpretation of these fluorescent emitters.

Toward Gas-Phase Ion Sensing. An aspect that remains undemonstrated here is the capture of Ba^{2+} within an environment of high-pressure xenon gas. Our past theoretical work[65] demonstrated that solvation-like effects with xenon are expected, with the shell configuration depending on gas temperature and pressure. The xenon shell typically contains 7−10 xenon atoms for Ba^{2+} at 10−15 bar. Capture by a molecular layer must free Ba^{2+} from this shell of accompanying spectator atoms, typically held at a binding energy of 3−4 eV. The Ba^{2+} binding energy of the molecules developed in this work is calculated to be around 0.2 eV in MeCN. However, calculations of the binding affinity in the gas phase, removing polarization effects of the solvent, show a much enhanced binding energy of −10.5 eV. This is sufficient to extract the target Ba^{2+} from its weakly attached xenon neighbors, so efficient capture of Ba^{2+} from high-pressure xenon gas is expected. Notably, the xenon solvation shell may also offer useful protection until proximity adequate for capture occurs.

A pertinent question for design of a molecular sensing layer at the gas−solid interface is the optimal surface density of probe molecules. An ultradense fluorophore layer is likely to suffer from collective quenching effects, whereas an overly sparse one may not efficiently capture arriving ions. To this end, we undertook computations of the range of ion capture. Complexation can be considered to be inevitable when the ion−molecule proximity is such that the binding energy is more than a few times the thermal energy ($kT \sim 0.02$ eV at STP). To evaluate the effective capture range, the most stable geometry of the complex **1B−Ba^{2+}** was evaluated as a function of ion-to-surface distance in the gas phase (Figure 8). Upon

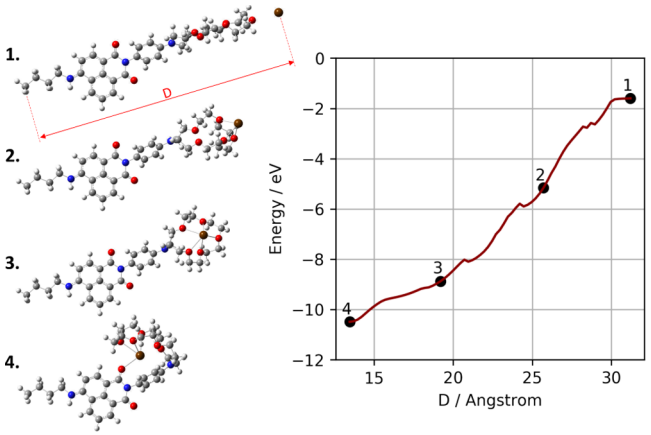

Figure 8. Simulation of ionic capture (left) and the potential energy surface in the gas phase as a function of ion-to-surface distance (right).

allowing Ba^{2+} to move closer to the azacrown ether surface, a bent geometry was obtained where the ion is bound to naphthalimide oxygen along with four ethereal oxygen atoms of the azacrown ether substructure (structure 4). This bent geometry of the complex is consistent with the NMR titration study in solution, in which the nitrogen atom of the azacrown ether did not appear to directly bind with the electron-withdrawing Ba^{2+} ion.

Beyond a range of 32 Å from the anchor point, our simulations fail to converge. The binding energy at this distance is still large, at 1.75 eV. Extrapolating the trend observed in the potential energy surface, it appears that the effective binding range of the molecule is somewhere between 32 and 40 Å. This suggests a range of densities for future monolayer construction, in order to realize efficient binding and reduce intermolecular distortions to fluorescent events. Exploration of the power of sensitive, semidense monolayers for ion capture at the solid−gas interface is the next immediate step in this ongoing program.

CONCLUSIONS

We have designed, synthesized, and studied barium-selective fluorescent sensors capable of ion sensing in dry environments, specifically selective Ba^{2+} imaging via SMFI. We found that a new, convenient, and visible-spectrum 4-amino-1,8-naphthalimide derivative with a diaza-18-crown-6 binding domain dramatically improved the selectivity of the sensors to Ba^{2+} without significantly compromising sensitivity. Solution-phase fluorescence and NMR experiments supported a PET mechanism enabling turn-on fluorescence sensing in the presence of metal ions. Experiments showed strong binding of Ba^{2+} to the sensor with 1:1 stoichiometry and a nanomolar LOD. Experimentally validated theoretical calculations illuminated the mechanism of fluorescence sensing, in addition to providing insights into the expected behavior at gas−solid interfaces.

SMFI microscopy in the air-coupled epifluorescent mode was employed for sensing of single Ba^{2+} ions with these fluorophores. Cyanoacrylate was found to be an effective support medium for the aforementioned fluorophores, and because of the sensor's strong selectivity for barium, no competitive binding agent was required to achieve single-molecule sensitivity with these molecules. Single-Ba^{2+} candidates were resolved spatially and identified through single-step photobleaching transitions, with enhanced prevalence in barium-washed samples. Realization of single-Ba^{2+} sensitivity under these conditions represents an important step toward practical application of this technique within time projection chambers. Such a technique could enable new precision and robustness in searches for $0\nu\beta\beta$ in xenon gas.

ASSOCIATED CONTENT

Supporting Information

The Supporting Information is available free of charge at https://pubs.acs.org/doi/10.1021/acssensors.0c02104.

Synthetic procedures, NMR spectral data and figures, UV−vis spectra, fluorescent titration, NMR titration spectral figures, and solid-phase fluorescent response of molecular probes (PDF)

AUTHOR INFORMATION

Corresponding Authors

Pawan Thapa − *Department of Chemistry and Biochemistry, University of Texas at Arlington, Arlington, Texas 76019, United States; Department of Physics, University of Texas at Arlington, Arlington, Texas 76019, United States;* Email: pawan.thapa@uta.edu

Nicholas K. Byrnes − *Department of Physics, University of Texas at Arlington, Arlington, Texas 76019, United States;* Email: byrnes.nicholas@mavs.uta.edu

https://dx.doi.org/10.1021/acssensors.0c02104
ACS Sens. 2021, 6, 192−202

Benjamin J. P. Jones − *Department of Physics, University of Texas at Arlington, Arlington, Texas 76019, United States*; Email: ben.jones@uta.edu

Frank W. Foss, Jr. − *Department of Chemistry and Biochemistry, University of Texas at Arlington, Arlington, Texas 76019, United States*; orcid.org/0000-0003-1940-6580; Email: ffoss@uta.edu

Authors

Alena A. Denisenko − *Department of Chemistry and Biochemistry, University of Texas at Arlington, Arlington, Texas 76019, United States*

James X. Mao − *Department of Chemistry and Biochemistry, University of Texas at Arlington, Arlington, Texas 76019, United States*

Austin D. McDonald − *Department of Physics, University of Texas at Arlington, Arlington, Texas 76019, United States*

Charleston A. Newhouse − *Department of Chemistry and Biochemistry, University of Texas at Arlington, Arlington, Texas 76019, United States*

Thanh T. Vuong − *Department of Chemistry and Biochemistry, University of Texas at Arlington, Arlington, Texas 76019, United States*

Katherine Woodruff − *Department of Physics, University of Texas at Arlington, Arlington, Texas 76019, United States*

Kwangho Nam − *Department of Chemistry and Biochemistry, University of Texas at Arlington, Arlington, Texas 76019, United States*; orcid.org/0000-0003-0723-7839

David R. Nygren − *Department of Physics, University of Texas at Arlington, Arlington, Texas 76019, United States*

Complete contact information is available at: https://pubs.acs.org/10.1021/acssensors.0c02104

Notes

The authors declare no competing financial interest.

■ ACKNOWLEDGMENTS

This work was undertaken as part of an ongoing interdisciplinary program to develop barium-tagging technologies for the NEXT experiment. We gratefully acknowledge support from the Department of Energy under awards DE-SC0019054 and DE-SC0019223, from the National Science Foundation under award CHE-2004111, from the Robert A. Welch Foundation, and from the University of Texas at Arlington. NMR experimentation was made possible by the National Science Foundation under award CHE-0840509. Mass spectrometry experiments were completed in the Shimadzu Center for Analytical Chemistry at UT Arlington.

■ REFERENCES

(1) Fukugita, M.; Yanagida, T. Baryogenesis Without Grand Unification. *Phys. Lett. B* **1986**, *174*, 45−47.

(2) Moe, M. K. New approach to the detection of neutrinoless double beta decay. *Phys. Rev. C: Nucl. Phys.* **1991**, *44*, 931−934.

(3) Chambers, C.; Walton, T.; Fairbank, D.; Craycraft, A.; Yahne, D.; Todd, J.; Iverson, A.; Fairbank, W.; Alamre, A.; Albert, J.; et al. Imaging individual barium atoms in solid xenon for barium tagging in nEXO. *Nature* **2019**, *569*, 203.

(4) McDonald, A. D.; Jones, B. J. P.; Nygren, D. R.; Adams, C.; Álvarez, V.; Azevedo, C. D. R.; Benlloch-Rodríguez, J. M.; Borges, F. I. G. M.; Botas, A.; Cárcel, S.; et al. Demonstration of single-barium-ion sensitivity for neutrinoless double-beta decay using single-molecule fluorescence imaging. *Phys. Rev. Lett.* **2018**, *120*, 132504.

(5) Nygren, D. R. Detection of the barium daughter in ^{136}Xe ^{136}Ba + 2e- by in situ single-molecule fluorescence imaging. *Nucl. Instrum. Methods Phys. Res., Sect. A* **2016**, *824*, 2.

(6) Jones, B. J. P.; McDonald, A. D.; Nygren, D. R. Single molecule fluorescence imaging as a technique for barium tagging in neutrinoless double beta decay. *J. Instrum.* **2016**, *11*, P12011.

(7) De Silva, A. P.; Gunaratne, H. Q. N.; Gunnlaugsson, T.; Huxley, A. J. M.; McCoy, C. P.; Rademacher, J. T.; Rice, T. E. Signaling recognition events with fluorescent sensors and switches. *Chem. Rev.* **1997**, *97*, 1515−1566.

(8) Valeur, B.; Leray, I. Design principles of fluorescent molecular sensors for cation recognition. *Coord. Chem. Rev.* **2000**, *205*, 3−40.

(9) Hamilton, G. R. C.; Sahoo, S. K.; Kamila, S.; Singh, N.; Kaur, N.; Hyland, B. W.; Callan, J. F. Optical probes for the detection of protons, and alkali and alkaline earth metal cations. *Chem. Soc. Rev.* **2015**, *44*, 4415−4432.

(10) Duke, R. M.; Veale, E. B.; Pfeffer, F. M.; Kruger, P. E.; Gunnlaugsson, T. Colorimetric and fluorescent anion sensors: an overview of recent developments in the use of 1,8-naphthalimide-based chemosensors. *Chem. Soc. Rev.* **2010**, *39*, 3936−3953.

(11) Panchenko, P. A.; Fedorova, O. A.; Fedorov, Y. V. Fluorescent and colorimetric chemosensors for cations based on 1,8-naphthalimide derivatives: design principles and optical signalling mechanisms. *Russ. Chem. Rev.* **2014**, *83*, 155.

(12) Panchenko, P. A.; Fedorov, Y. V.; Fedorova, O. A.; Jonusauskas, G. Comparative analysis of the PET and ICT sensor properties of 1,8-naphthalimides containing aza-15-crown-5 ether moiety. *Dyes Pigm.* **2013**, *98*, 347−357.

(13) Gao, Z.; Hao, Y.; Zheng, M.; Chen, Y. A fluorescent dye with large Stokes shift and high stability: synthesis and application to live cell imaging. *RSC Adv.* **2017**, *7*, 7604−7609.

(14) Alfimov, M.; Gromov, S. *Applied Fluorescence in Chemistry, Biology and Medicine*; Springer, 1999; pp 161−178.

(15) Hou, C.; Urbanec, A. M.; Cao, H. A rapid Hg^{2+} sensor based on aza-15-crown-5 ether functionalized 1,8-naphthalimide. *Tetrahedron Lett.* **2011**, *52*, 4903−4905.

(16) Panchenko, P. A.; Park, V. V.; Fedorova, O. A.; Fedorov, Y. V.; Kataev, E. A. Cation-dependent spectral properties of fluorescent complexon based on 1,8-naphthalimide with PET mechanism of optical response. *Russ. Chem. Bull.* **2015**, *64*, 1871−1876.

(17) Panchenko, P. A.; Fedorov, Y. V.; Fedorova, O. A. Selective fluorometric sensing of Hg^{2+} in aqueous solution by the inhibition of PET from dithia-15-crown-5 ether receptor conjugated to 4-amino-1,8-naphthalimide fluorophore. *J. Photochem. Photobiol., A* **2018**, *364*, 124−129.

(18) Panchenko, P. A.; Polyakova, A. S.; Fedorov, Y. V.; Fedorova, O. A. Chemoselective detection of Ag^{+} in purely aqueous solution using fluorescence 'turn-on'probe based on crown-containing 4-methoxy-1,8-naphthalimide. *Mendeleev Commun.* **2019**, *29*, 155−157.

(19) Georgiev, N. I.; Dimitrova, M. D.; Todorova, Y. D.; Bojinov, V. B. Synthesis, chemosensing properties and logic behaviour of a novel ratiometric 1,8-naphthalimide probe based on ICT and PET. *Dyes Pigm.* **2016**, *131*, 9−17.

(20) Fernández-Alonso, S.; Corrales, T.; Pablos, J. L.; Catalina, F. Solid fluorescence sensors obtained by functionalization of photo-crosslinked water-swollen acrylic membranes with 4-piperazine naphthalimide derivatives. *Polymer* **2017**, *124*, 139−150.

(21) Aderinto, S. O.; Zhang, H.; Wu, H.; Chen, C.; Zhang, J.; Peng, H.; Yang, Z.; Wang, F. Synthesis and studies of two proton−receptor fluorescent probes based on 1,8-naphthalimide. *Color. Technol.* **2017**, *133*, 40−49.

(22) Georgiev, N. I.; Krasteva, P. V.; Bojinov, V. B. A ratiometric 4-amido-1,8-naphthalimide fluorescent probe based on excimer-monomer emission for determination of pH and water content in organic solvents. *J. Lumin.* **2019**, *212*, 271−278.

(23) Licchelli, M.; Orbelli Biroli, A.; Poggi, A. A prototype for the chemosensing of Ba^{2+} based on self-assembling fluorescence enhancement. *Org. Lett.* **2006**, *8*, 915−918.

(24) Patnaik, P. *Handbook of Inorganic Chemicals*; McGraw-Hill: New York, 2003; Vol. *529*.
(25) Zhao, J.-M.; Zong, Q.-S.; Chen, C.-F. Complexation of triptycene-based macrotricyclic host toward (9-anthracylmethyl) benzylammonium salt: a Ba^{2+} selective fluorescence probe. *J. Org. Chem.* **2010**, *75*, 5092−5098.
(26) Saluja, P.; Kaur, N.; Singh, N.; Jang, D. O. A benzthiazole-based tripodal chemosensor for Ba^{2+} recognition under biological conditions. *Tetrahedron Lett.* **2011**, *52*, 6705−6708.
(27) Banerjee, T.; Suresh, M.; Ghosh, H. N.; Das, A. Competitive binding of Ba^{2+} and Sr^{2+} to 18-Crown-6 in a Receptor with a 1-Methoxyanthraquinone Analogue as the Other Binding Site. *Eur. J. Inorg. Chem.* **2011**, *2011*, 4680−4690.
(28) Basa, P. N.; Bhowmick, A.; Schulz, M. M.; Sykes, A. G. Site-selective imination of an anthracenone sensor: selective fluorescence detection of barium (II). *J. Org. Chem.* **2011**, *76*, 7866−7871.
(29) Guo, H.; Kuwabara, T. Colorimetric Chemosensor for Barium Metal Ions Using Tris (bipyridinium−crown ether) Conjugate. *Chem. Lett.* **2013**, *42*, 194−196.
(30) García Grajeda, B. A.; Soto Acosta, S. G.; Aguila, S. A.; Peinado Guevara, H.; Díaz García, M. E.; Cruz Enríquez, A.; Campos Gaxiola, J. J. Selective and colorimetric detection of Ba^{2+} ions in aqueous solutions using 11-mercaptoundecylphosphonic acid functionalized gold nanoparticles. *RSC Adv.* **2017**, *7*, 31611.
(31) Chaichana, K.; Phutlaprungrueang, N.; Chaicharoenwimolkul, L.; Promkatkaew, M.; Kongsriprapan, S. A selective fluorescence probe based on naphthalene for the detection of barium(II). *Spectrochim. Acta, Part A* **2019**, *207*, 118−122.
(32) Li, F.; Zhong, K.; Hou, S.; Tang, L.; Bian, Y. A simple and efficient fluorescent probe for detecting Ba^{2+} and its various applications. *Tetrahedron Lett.* **2020**, *61*, 151558.
(33) Kravchenko, J.; Darrah, T. H.; Miller, R. K.; Lyerly, H. K.; Vengosh, A. A review of the health impacts of barium from natural and anthropogenic exposure. *Environ. Geochem. Health* **2014**, *36*, 797−814.
(34) Łukasik-Głębocka, M.; Sommerfeld, K.; Hanć, A.; Grzegorowski, A.; Barałkiewicz, D.; Gaca, M.; Zielińska-Psuja, B. Barium determination in gastric contents, blood and urine by inductively coupled plasma mass spectrometry in the case of oral barium chloride poisoning. *J. Anal. Toxicol.* **2014**, *38*, 380−382.
(35) Nakahara, Y.; Kida, T.; Nakatsuji, Y.; Akashi, M. A novel fluorescent indicator for Ba^{2+} in aqueous micellar solutions. *Chem. Commun.* **2004**, 224−225.
(36) Nakahara, Y.; Kida, T.; Nakatsuji, Y.; Akashi, M. Fluorometric sensing of alkali metal and alkaline earth metal cations by novel photosensitive monoazacryptand derivatives in aqueous micellar solutions. *Org. Biomol. Chem.* **2005**, *3*, 1787−1794.
(37) Thapa, P.; Arnquist, I.; Byrnes, N.; Denisenko, A.; Foss, F.; Jones, B.; McDonald, A.; Nygren, D.; Woodruff, K. Barium chemosensors with Dry-phase fluorescence for neutrinoless Double Beta Decay. *Sci. Rep.* **2019**, *9*, 15097.
(38) Kondo, S.-i.; Takahashi, T.; Takiguchi, Y.; Unno, M. Synthesis and photophysical properties of a 2, 2′-bianthracene-based receptor bearing two aza-15-crown-5 ethers for naked-eye detection of barium ion. *Tetrahedron Lett.* **2011**, *52*, 453−457.
(39) Yang, C.; Liu, L.; Zeng, T.; Yang, D.; Yao, Z.; Zhao, Y.; Wu, H.-C. Highly sensitive simultaneous detection of lead (II) and barium (II) with G-quadruplex DNA in α-hemolysin nanopore. *Anal. Chem.* **2013**, *85*, 7302−7307.
(40) Xu, L.; Chen, Y.; Zhang, R.; Gao, T.; Zhang, Y.; Shen, X.; Pei, R. A highly Sensitive Turn-on Fluorescent Sensor for Ba^{2+} Based on G-Quadruplexes. *J. Fluoresc.* **2017**, *27*, 569−574.
(41) Ravichandiran, P.; Subramaniyan, S. A.; Bella, A. P.; Johnson, P. M.; Kim, A. R.; Shim, K. S.; Yoo, D. J. Simple fluorescence turn-on chemosensor for selective detection of Ba^{2+} ion and its live cell imaging. *Anal. Chem.* **2019**, *91*, 10095−10101.
(42) Monrabal, F.; Gómez-Cadenas, J. J.; Toledo, J. F.; Laing, A.; Álvarez, V.; Benlloch-Rodríguez, J. M.; Cárcel, S.; Carrión, J. V.; Esteve, R.; Felkai, R.; et al. The next white (new) detector. *J. Instrum.* **2018**, *13*, P12010.
(43) Martín-Albo, J.; Vidal, J. M.; Ferrario, P.; Nebot-Guinot, M.; Gómez-Cadenas, J.; Álvarez, V.; Azevedo, C.; Borges, F.; Cárcel, S.; Carrión, J.; et al. Sensitivity of NEXT-100 to neutrinoless double beta decay. *J. High Energy Phys.* **2016**, *2016*, 159.
(44) Adams, C.; Alvarez, V.; Arazi, L.; Arnquist, I.; Azevedo, C.; Bailey, K.; Ballester, F.; Benlloch-Rodriguez, J.; Borges, F.; Byrnes, N.; et al. Sensitivity of a tonne-scale NEXT detector for neutrinoless double beta decay searches, **2020**. arXiv:2005.06467, https://arxiv.org/abs/2005.06467, (accessed on Dec 18, 2020).
(45) Rivilla, I.; Aparicio, B.; Bueno, J. M.; Casanova, D.; Tonnelé, C.; Freixa, Z.; Herrero, P.; Rogero, C.; Miranda, J. I.; Martínez-Ojeda, R. M.; et al. Fluorescent bicolour sensor for low-background neutrinoless double β decay experiments. *Nature* **2020**, *583*, 48−54.
(46) Luk'yanenko, N. G.; Basok, S.; Kulygina, E. Y.; Bogashchenko, T. Y.; Yakovenko, I. Synthesis of monoazacrown ethers under phase-transfer catalysis. *Russ. J. Org. Chem.* **2012**, *48*, 1345−1352.
(47) Koonrugsa, N.; Fuangswasdi, S. Metal ion chemosensors based on diaza-18-crown-6 coupling with azobenzene dye. *Spectrochim. Acta, Part A* **2019**, *215*, 15−23.
(48) Zhao, Y.; Truhlar, D. G. The M06 suite of density functionals for main group thermochemistry, thermochemical kinetics, noncovalent interactions, excited states, and transition elements: two new functionals and systematic testing of four M06-class functionals and 12 other functionals. *Theor. Chem. Acc.* **2008**, *120*, 215−241.
(49) Dolg, M.; Wedig, U.; Stoll, H.; Preuss, H. Energy-adjusted abinitio pseudopotentials for the first row transition elements. *J. Chem. Phys.* **1987**, *86*, 866−872.
(50) Kaupp, M.; Schleyer, P. v. R.; Stoll, H.; Preuss, H. Pseudopotential approaches to Ca, Sr, and Ba hydrides. Why are some alkaline earth MX2 compounds bent? *J. Chem. Phys.* **1991**, *94*, 1360−1366.
(51) Bergner, A.; Dolg, M.; Küchle, W.; Stoll, H.; Preuß, H. Ab initio energy-adjusted pseudopotentials for elements of groups 13−17. *Mol. Phys.* **1993**, *80*, 1431−1441.
(52) Dolg, M.; Stoll, H.; Preuss, H.; Pitzer, R. M. Relativistic and correlation effects for element 105 (hahnium, Ha): a comparative study of M and MO (M= Nb, Ta, Ha) using energy-adjusted ab initio pseudopotentials. *J. Phys. Chem.* **1993**, *97*, 5852−5859.
(53) Weigend, F.; Ahlrichs, R. Balanced basis sets of split valence, triple zeta valence and quadruple zeta valence quality for H to Rn: Design and assessment of accuracy. *Phys. Chem. Chem. Phys.* **2005**, *7*, 3297−3305.
(54) Weigend, F. Accurate Coulomb-fitting basis sets for H to Rn. *Phys. Chem. Chem. Phys.* **2006**, *8*, 1057−1065.
(55) Runge, E.; Gross, E. K. U. Density-functional theory for time-dependent systems. *Phys. Rev. Lett.* **1984**, *52*, 997.
(56) Marenich, A. V.; Cramer, C. J.; Truhlar, D. G. Universal solvation model based on solute electron density and on a continuum model of the solvent defined by the bulk dielectric constant and atomic surface tensions. *J. Phys. Chem. B* **2009**, *113*, 6378−6396.
(57) Hall, R. J.; Davidson, M. M.; Burton, N. A.; Hillier, I. H. Combined density functional, self-consistent reaction field model of solvation. *J. Phys. Chem.* **1995**, *99*, 921−924.
(58) Frisch, M. J.; Trucks, G. W.; Schlegel, H. B.; Scuseria, G. E.; Robb, M. A., Jr.; Cheeseman, G.; Scalmani, V.; Barone, B.; Mennucci, G. A.; Petersson, H.; et al. *Gaussian 09*, R. A. 1; Gaussian Inc.: Wallingford CT, 2009.
(59) Fabbrizzi, L.; Licchelli, M.; Pallavicini, P.; Perotti, A.; Taglietti, A.; Sacchi, D. Fluorescent sensors for transition metals based on electron-transfer and energy-transfer mechanisms. *Chem.—Eur. J.* **1996**, *2*, 75−82.
(60) Callan, J. F.; de Silva, A. P.; Magri, D. C. Luminescent sensors and switches in the early 21st century. *Tetrahedron* **2005**, *61*, 8551−8588.
(61) Veale, E. B.; Kitchen, J. A.; Gunnlaugsson, T. Fluorescent tren-based 4-amino-1,8-naphthalimide sensor for Cu (II) based on the use

of the (fluorophore−spacer−receptor) photoinduced electron transfer (PET) principle. *Supramol. Chem.* **2013**, *25*, 101−108.
(62) Abdurahman, A.; Hele, T. J. H.; Gu, Q.; Zhang, J.; Peng, Q.; Zhang, M.; Friend, R. H.; Li, F.; Evans, E. W. Understanding the luminescent nature of organic radicals for efficient doublet emitters and pure-red light-emitting diodes. *Nat. Mater.* **2020**, *19*, 1224−1229.
(63) Wang, L.; Qin, W.; Tang, X.; Dou, W.; Liu, W.; Teng, Q.; Yao, X. A selective, cell-permeable fluorescent probe for Al^{3+} in living cells. *Org. Biomol. Chem.* **2010**, *8*, 3751−3757.
(64) Lee, H.; Lee, H.-S.; Reibenspies, J. H.; Hancock, R. D. Mechanism of "turn-on" fluorescent sensors for mercury (II) in solution and its implications for ligand design. *Inorg. Chem.* **2012**, *51*, 10904−10915.
(65) Bainglass, E.; Jones, B. P.; Foss, F.; Huda, M.; Nygren, D. Mobility and Clustering of Barium Ions and Dications in High Pressure Xenon Gas. *Phys. Rev. A* **2018**, *97*, 062509.

https://dx.doi.org/10.1021/acssensors.0c02104
ACS Sens. 2021, 6, 192−202